3-DIMENSIONAL IMPLEMENTATION OF THE FIELD ITERATIVE METHOD FOR CAVITY MODELING

C.-F. Wang, Y. Xu, and Y.-B. Gan

Temasek Laboratories
National University of Singapore
10 Kent Ridge Crescent, Singapore 119260

Abstract—The analysis of electromagnetic scattering from cavity structure is very important to many practical applications. The field iterative method (FIM) is one of the promising methods to deal with the cavity problem. In this paper, 3-dimensional (3D) FIM has been implemented using Rao-Wilton-Glisson (RWG) basis function and an accurate equivalent model of the cavity. Two testing procedures, a newly developed point matching and conventional Galerkin's methods, have been discussed for better and simpler implementation of the 3D FIM. Numerical results show that the accuracy of the 3D implementation of FIM using the newly developed point matching method is the same as that of the conventional Galerkin's method. The numerical results also show that the simpler implementation of 3D FIM using the point matching method converges very fast for all the tested cases.

1. INTRODUCTION

Electromagnetic modeling of open cavities is a problem of fundamental importance in the reduction of back and forward scattering, as well as electromagnetic penetration studies. It is well known that scattering from the interior of the jet engine inlet cavities contributes significantly to the overall back scattering of an aircraft. The first technique used to analyze cavity structure is the generalized network formulation (GNF) proposed by Harrington and Mautz [1]. The GNF decomposes the scattering domain into two parts (i.e., an infinite half space and a cavity) which are connected via currents on the fictitious surface between the cavity and half space. However, the integral equation for the closed domain bounded by an actually physical cavity wall and the fictitious surface separating the cavity from the half space is plagued by the usual problem of non-uniqueness at the cavity resonant frequency [2]. In this approach, the interior and exterior fields of the cavity are coupled by a fictitious magnetic current on the interface between the cavity and free space. The virtue of this method is its relatively simplicity; however, the price one pays is the appearance of spurious resonance.

For very large cavities, high-frequency techniques based on ray-tracing and edge diffraction can be employed to evaluate the scattering pattern. These include the shooting and bouncing ray (SBR) method [3], the generalized ray expansion (GRE) method [4], and the iterative physical optics (IPO) method [5]. These approaches are promising for cavity with simple interior geometry. An efficient approach based on the finite element-boundary integral (FE-BI) method was proposed to model cavity structures in [6, 7]. Recently, the FE-BI method has been extended to simulate the scattering from very large and complex cavity structures [8–10]. Another method for cavity modeling is a connection scheme that was proposed using microwave network theory to reduce both CPU time and memory requirement [11, 12].

As described in [13], the cavity problem, such as the electromagnetic scattering from a jet engine, may be visualized as consisting of three distinct phenomena: 1) an aperture field that is established from the external region source; 2) the electric and magnetic fields that propagate down the cavity, guided by the cavity walls; and 3) reflection that occurs at the termination. Upon reflection, the fields propagate back towards the aperture where they may be integrated to give the far zone scattered field. Based on the field propagation in the cavity, the field iterative method (FIM) [13] was proposed to describe the propagation of the field from the aperture to the termination and back to the aperture. Unfortunately, there are

some errors in the original paper [13]. The FIM was carefully studied in [14–16]. An accurate equivalent model of cavity for the FIM was proposed in [15, 16]. The FIM based on the accurate equivalent model of the cavity was implemented for 2-dimensional (2D) cavity problem to verify the method. Good accuracy and convergence behaviour of the FIM was observed for all 2D test cases. All simulation results can be considered as benchmarks for 2D cavity modeling using the FIM [15].

In this paper, the 3-dimensional (3D) FIM has been implemented using the Rao-Wilton-Glisson (RWG) basis functions [17] to fit the shape of cavity and the accurate equivalent model of cavity [15, 16] to guarantee the accuracy of the FIM. Two testing procedures, i.e., a newly developed point matching and the conventional Galerkin's methods, will be discussed for better and simpler implementation of the 3D FIM. Numerical results show that the accuracy of the 3D implementation of the FIM using the newly developed point matching method is the same as that of the conventional Galerkins method. The numerical results also show that the simpler implementation of the 3D FIM based on the point matching method converges very fast for all test cases.

2. THEORY AND FORMULATIONS FOR FIM

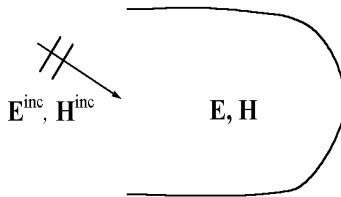### 2.1. Integral Equations for FIM

Figure 1. Cavity illuminated by an external plane wave.

Consider the problem as shown in Fig. 1. Here, an incident plane wave illuminates part of the external cavity walls and the aperture. The total scattered field consists of two parts, $\mathbf{E}^s = \mathbf{E}^s_{cav} + \mathbf{E}^s_{ext}$, where $\mathbf{E}^s_{cav}$ is the contribution from the interior of the cavity and $\mathbf{E}^s_{ext}$ is the contribution from the external surface, including the scattering from the rim edge of the aperture at the open end. The aim of this research is to study the internal scattering problem without consideration on the scattering due to the external surface. Thus, we actually consider
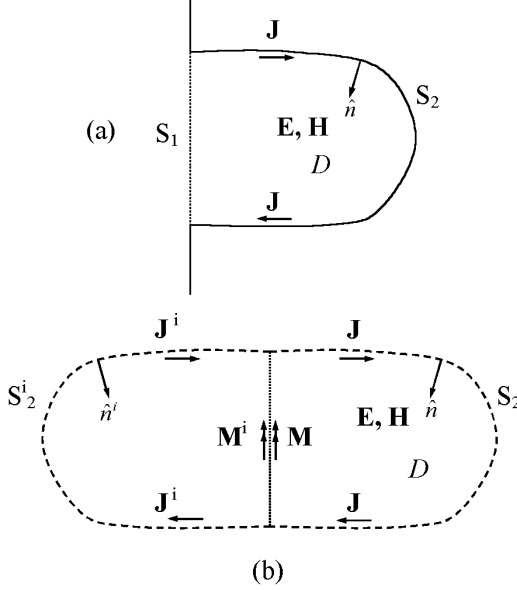
Figure 2. (a) The modified problem, (b) An accurate equivalent model of the cavity problem.

the problem shown in Fig. 2(a), where $\hat{n}$ is the unit surface normal vector pointing into the cavity. S_1 and S_2 denote aperture surface and cavity interior surface, respectively, and D denotes the cavity region enclosed by S_1 and S_2. By using the equivalent principle and image theory [18], an accurate equivalent model of cavity can be established as shown in Fig. 2(b) [15, 16].

The total magnetic field due to the presence of both electric and magnetic currents can be written as [19],

$$\mathbf{H}(\mathbf{r}) = \int_S \mathbf{J}(\mathbf{r}') \times \nabla' G(\mathbf{r}, \mathbf{r}') ds' - \frac{j}{k_0 Z_0} \left\{ k_0^2 \int_S G(\mathbf{r}, \mathbf{r}') \mathbf{M}(\mathbf{r}') ds' \right.$$
$$\left. + \int_S \nabla' \nabla' G(\mathbf{r}, \mathbf{r}') \cdot \mathbf{M}(\mathbf{r}') ds' \right\}, \quad \mathbf{r} \in D \tag{1}$$

where $S = S_1 + S_2 + S_2^i$, and $G(\mathbf{r}, \mathbf{r}')$ is the free space Green's functions. Applying the boundary conditions on the walls and aperture of the cavity leads to

$$\mathbf{H}(\mathbf{r}) = \int_{S_2} \mathbf{J}(\mathbf{r}') \times \nabla' G(\mathbf{r}, \mathbf{r}') ds' + \int_{S_2^i} \mathbf{J}^i(\mathbf{r}') \times \nabla' G(\mathbf{r}, \mathbf{r}') ds'$$

$$-\frac{2j}{k_0 Z_0}\left\{k_0^2 \int_{S_1} G(\mathbf{r},\mathbf{r}')\mathbf{M}(\mathbf{r}')ds'\right.$$

$$\left. -\int_{S_1}\nabla' G(\mathbf{r},\mathbf{r}')\nabla'\cdot\mathbf{M}(\mathbf{r}')ds'\right\},\quad \mathbf{r}\in D \tag{2}$$

To obtain the integral equations governing the currents, the following equation is used,

$$\lim_{\mathbf{r}''\to\mathbf{r}}\hat{n}(\mathbf{r})\times\int_S\mathbf{J}(\mathbf{r}')\times\nabla' G(\mathbf{r}'',\mathbf{r}')ds'$$

$$=\frac{1}{2}\mathbf{J}(\mathbf{r})+\hat{n}\times\int_S\mathbf{J}(\mathbf{r}')\times\nabla' G(\mathbf{r},\mathbf{r}')ds'\quad \mathbf{r}''\in D,\quad \mathbf{r}\in S_2 \tag{3}$$

where the integral on the right hand side of equation (3) implies the principal value of the integration. Eq. (3) can be established from the evaluation of the residue of a divergent integral for scalar wave [20] (see Appendix A).

With equation (3) and the equivalent electric current $\mathbf{J}=\hat{n}\times\mathbf{H}$, after moving the field point $\mathbf{r}$ to S_2, we obtained the final magnetic field integral equation (MFIE),

$$\mathbf{J}(\mathbf{r}) = \frac{1}{2}\mathbf{J}(\mathbf{r})+\hat{n}\times\int_{S_2}\mathbf{J}(\mathbf{r}')\times\nabla' G(\mathbf{r},\mathbf{r}')ds'$$

$$+\hat{n}\times\int_{S_2^i}\mathbf{J}^i(\mathbf{r}')\times\nabla' G(\mathbf{r},\mathbf{r}')ds'$$

$$-\frac{2j}{k_0 Z_0}\left\{k_0^2\hat{n}\times\int_{S_1}G(\mathbf{r},\mathbf{r}')\mathbf{M}(\mathbf{r}')ds'\right.$$

$$\left.-\hat{n}\times\int_{S_1}\nabla' G(\mathbf{r},\mathbf{r}')\nabla'\cdot\mathbf{M}(\mathbf{r}')ds'\right\},\quad \mathbf{r}\in S_2 \tag{4}$$

where the first integral in equation (4) implies the principal value of the integration along S_2. An equation for the scattered field at the aperture of the cavity can be written using the electric field integral equations (EFIE) as [15, 16],

$$\mathbf{E}^{scat}(\mathbf{r})=-\frac{jZ_0}{k_0}\left\{k_0^2\int_{S_2}G(\mathbf{r},\mathbf{r}')\mathbf{J}(\mathbf{r}')ds'-\int_{S_2}\nabla' G(\mathbf{r},\mathbf{r}')\nabla'\cdot\mathbf{J}(\mathbf{r}')ds'\right\}$$

Using $\mathbf{M}^{scat}=\mathbf{E}^{scat}\times\hat{n}$, we obtain the final EFIE,

$$\mathbf{M}^{scat}(\mathbf{r}) = -\frac{jZ_0}{k_0}\left\{k_0^2\int_{S_2}G(\mathbf{r},\mathbf{r}')\mathbf{J}(\mathbf{r}')\times\hat{n}ds'\right.$$

$$\left.-\int_{S_2}\nabla' G(\mathbf{r},\mathbf{r}')\times\hat{n}\nabla'\cdot\mathbf{J}(\mathbf{r}')ds'\right\},\quad \mathbf{r}\in S_1 \tag{5}$$

Equations (4) and (5) can be implemented numerically by expanding the electric and magnetic currents into series of basis functions on the cavity walls and the aperture of the cavity, respectively. To fit the arbitrary shape of the cavity, the RWG vector basis functions [17] are chosen to approximate the electric and magnetic currents, respectively. Assuming that there are N basis functions on the cavity wall S_2 and P basis functions on the aperture S_1, namely,

$$\mathbf{J}(\mathbf{r}') \;\; = \;\; \sum_{n=1}^{N} H_n \mathbf{f}_n(\mathbf{r}') \quad \mathbf{r}' \in S_2 \tag{6}$$

$$\mathbf{M}(\mathbf{r}') \;\; = \;\; \sum_{p=1}^{P} E_p \mathbf{g}_p(\mathbf{r}') \quad \mathbf{r}' \in S_1 \tag{7}$$

$$\mathbf{M}^{scat}(\mathbf{r}') = \mathbf{E}^{scat}(\mathbf{r}') \times \hat{n} = \sum_{p=1}^{P} E_p^{scat} \mathbf{g}_p(\mathbf{r}') \quad \mathbf{r}' \in S_1 \tag{8}$$

where $\mathbf{f}_n$, $\mathbf{g}_p$ are RWG vector basis functions on S_1 and S_2, respectively. As mentioned in [13–16], the standard procedure of method of moments (MoM) can discretize the equations (3) and (4) into linear systems of equations [17, 21]. For the testing procedure, the conventional Galerkin's and point matching methods can be applied to obtain different FIM formulations, which are worth discussing in detail.
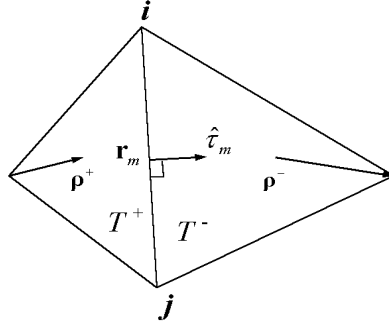
2.2. FIM Using Point Matching Method

Figure 3. The RWG basis function and its vector delta function.

For a given RWG basis function $\mathbf{f}_m$ as shown in Fig. 3, a vector delta function related to $\mathbf{f}_m$ can be defined as $\mathbf{t}_m = \delta(\mathbf{r} - \mathbf{r}_m)\hat{\tau}_m$, where $\mathbf{r}_m$ is the midpoint of edge $\{i, j\}$, $\hat{\tau}_m$ is a unit vector perpendicular to the edge and parallel to the plane of triangle T^+.

Substituting equations (6)–(8) into equations (4) and (5) gives rise to,

$$
\sum_{n=1}^{N} H_n \mathbf{f}_n(\mathbf{r}) = \frac{1}{2} \sum_{n=1}^{N} H_n \mathbf{f}_n(\mathbf{r}) + \sum_{n=1}^{N} H_n \left\{ \int_{S_2} \hat{n} \times (\mathbf{f}_n(\mathbf{r}') \right.
$$

$$
\times \nabla' G(\mathbf{r}, \mathbf{r}') ds' + \int_{S_2^i} \hat{n} \times (\mathbf{f}_n^i(\mathbf{r}_i') \times \nabla' G(\mathbf{r}, \mathbf{r}_i')) ds' \Bigg\}
$$

$$
- \frac{2j}{k_0 Z_0} \sum_{p=1}^{P} E_p \left\{ k_0^2 \hat{n} \times \int_{S_1} G(\mathbf{r}, \mathbf{r}') \mathbf{g}_p(\mathbf{r}') ds' \right.
$$

$$
\left. - \hat{n} \times \int_{S_1} \nabla' G(\mathbf{r}, \mathbf{r}') \nabla' \cdot \mathbf{g}_p(\mathbf{r}') ds' \right\} \quad \mathbf{r} \in S_2 \quad (9)
$$

$$
\sum_{p=1}^{P} E_p^{scat} \mathbf{g}_p(\mathbf{r}) = -\frac{jZ_0}{k_0} \sum_{m=1}^{N} H_m \left\{ k_0^2 \int_{S_2} G(\mathbf{r}, \mathbf{r}') \mathbf{f}_m(\mathbf{r}') \times \hat{n} ds' \right.
$$

$$
\left. - \int_{S_2} \nabla' G(\mathbf{r}, \mathbf{r}') \times \hat{n} \nabla' \cdot \mathbf{f}_m(\mathbf{r}') ds' \right\} \quad (10)
$$

Taking the inner products of both sides of equations (9) and (10) with vector delta function $\mathbf{t}_m$ results in the following equations

$$
H_m = \sum_{n=1}^{N} U_{mn} H_n + 2 \sum_{p=1}^{P} V_{mp} E_p, \quad m = 1, 2, \ldots, N \quad (11)
$$

$$
E_i^{scat} = \sum_{m=1}^{N} W_{im} H_m, \quad m = 1, 2, \ldots, P \quad (12)
$$

where

$$
U_{mn} = \begin{cases} \dfrac{1}{2} + \displaystyle\int_{S_2^i} \hat{\tau}_m \cdot \hat{n}_m \times (\mathbf{f}_n^i(\mathbf{r}_i') \times \nabla' G(\mathbf{r}_m, \mathbf{r}_i')) ds, & m = n \\[3mm] \displaystyle\int_{S_2} \hat{\tau}_m \cdot \hat{n}_m \times (\mathbf{f}_n(\mathbf{r}') \times \nabla' G(\mathbf{r}_m, \mathbf{r}_i')) ds' \\[3mm] \quad + \displaystyle\int_{S_2^i} \hat{\tau}_m \cdot \hat{n}_m \times (\mathbf{f}_n^i(\mathbf{r}_i') \times \nabla' G(\mathbf{r}_m, \mathbf{r}_i')) ds', & m \neq n \end{cases}
$$

$$
V_{mp} = -\frac{j}{k_0 Z_0} \left\{ k_0^2 \hat{\tau}_m \cdot \hat{n}_m \times \int_{S_1} G(\mathbf{r}_m, \mathbf{r}') \mathbf{g}_p(\mathbf{r}') ds' \right.
$$

$$
\left. - \hat{\tau}_m \cdot \hat{n}_m \times \int_{S_1} \nabla' G(\mathbf{r}_m, \mathbf{r}') \nabla' \cdot \mathbf{g}_p(\mathbf{r}') ds' \right\}
$$

$$
W_{im} = -\frac{jZ_0}{k_0} \left\{ k_0^2 \hat{\tau}_i \cdot \int_{S_2} G(\mathbf{r}_i, \mathbf{r}') \mathbf{f}_m(\mathbf{r}') ds' \times \hat{n}_i \right.
$$

$$-\hat{\tau}_i \cdot \int_{S_2} \nabla' G(\mathbf{r}_i, \mathbf{r}') \nabla' \cdot \mathbf{f}_m(\mathbf{r}') ds' \times \hat{n}_i \Big\}$$

where $\mathbf{r}'_i$ is the image of the source point $\mathbf{r}'$, $\mathbf{r}_m$ is the midpoint of the interior edge associated with the basis function $\mathbf{f}_m$, $\mathbf{r}_i$ is the midpoint of the interior edge associated with the basis function $\mathbf{g}_i$, $\mathbf{f}_n^i$ is the image of the basis function $\mathbf{f}_n$ with respect to the perfect electric conductor plane, $\hat{n}_m$, $\hat{n}_i$ are unit normal vectors at field points $\mathbf{r}_m$ and $\mathbf{r}_i$, which are chosen as the unit normal vectors of triangles T^+ in our numerical simulation. It is also noted that the total electric field at the aperture is given by the summation of the incident and scattered electric fields that can be discretized into the following equation

$$[E] = [E^{inc}] + [E^{scat}] \tag{13}$$

The above systems of linear equations (11)–(13) can be represented by the following matrix equations in the form of FIM

$$[H] = [U][H'] + [V][E] \tag{14}$$
$$[E^{scat}] = [W][H] \tag{15}$$
$$[E] = [E^{inc}] + [E^{scat}] \tag{16}$$

2.3. FIM Using Galerkin's Method

Applying Galerkin's method to equations (4), (5), and total electric field at the aperture results in the following equations, which are more complicated than equations (14)–(16),

$$\sum_{n=1}^{N} B_{mn} H_n = \sum_{n=1}^{N} U_{mn} H_n + 2 \sum_{p=1}^{P} V_{mp} E_p, \quad m = 1, 2, \cdots, N \tag{17}$$

$$\sum_{p=1}^{P} A_{ip} E_p^{scat} = \sum_{m=1}^{N} W_{im} H_m, \quad i = 1, 2, \cdots, P \tag{18}$$

$$\sum_{p=1}^{P} A_{ip} E_p = \tilde{E}_i^{inc} + \sum_{p=1}^{P} A_{ip} E_i^{scat}, \quad i = 1, 2, \cdots, P \tag{19}$$

where

$$A_{ip} = \int_{S_1} \mathbf{g}_p(\mathbf{r}) \cdot \mathbf{g}_i(\mathbf{r}) ds, \quad B_{mn} = \int_{S_2} \mathbf{f}_m(\mathbf{r}) \cdot \mathbf{f}_n(\mathbf{r}) ds$$

$$U_{mn} = \frac{1}{2} B_{mn} + \int_{S_2} \int_{S_2} \hat{n}_m(\mathbf{r}) \times (\mathbf{f}_n(\mathbf{r}') \times \nabla' G(\mathbf{r}, \mathbf{r}')) \cdot \mathbf{f}_m(\mathbf{r}) ds' ds$$

$$+ \int_{S_2} \int_{S_2^i} \hat{n}_m(\mathbf{r}) \times \left(\mathbf{f}_n^i(\mathbf{r}') \times \nabla' G(\mathbf{r}, \mathbf{r}_i') \right) \cdot \mathbf{f}_m(\mathbf{r}) ds' ds$$

$$V_{mp} = -\frac{j}{k_0 Z_0} \left[k_0^2 \int_{S_2} \int_{S_1} \hat{n}_m(\mathbf{r}) \times (G(\mathbf{r}, \mathbf{r}') \mathbf{g}_p(\mathbf{r}')) \cdot \mathbf{f}_m(\mathbf{r}) ds' ds \right.$$

$$\left. - \int_{S_2} \int_{S_1} \hat{n}_m(\mathbf{r}) \times (\nabla' G(\mathbf{r}, \mathbf{r}') \nabla' \cdot \mathbf{g}_p(\mathbf{r}')) \cdot \mathbf{f}_m(\mathbf{r}) ds' ds \right]$$

$$W_{im} = -\frac{jZ_0}{k_0} \left[k_0^2 \int_{S_1} \int_{S_2} (G(\mathbf{r}, \mathbf{r}') \mathbf{f}_m(\mathbf{r}') \times \hat{n}_i(\mathbf{r})) \cdot \mathbf{g}_i(\mathbf{r}) ds' ds \right.$$

$$\left. - \int_{S_1} \int_{S_2} (\nabla' G(\mathbf{r}, \mathbf{r}') \nabla' \cdot \mathbf{f}_m(\mathbf{r}') \times \hat{n}_i(\mathbf{r})) \cdot \mathbf{g}_i(\mathbf{r}) ds' ds \right]$$

$$\tilde{E}_i^{inc} = \int_{S_1} \mathbf{E}^{inc}(\mathbf{r}) \cdot \mathbf{g}_i(\mathbf{r}) ds$$

where $\hat{n}_m(\mathbf{r})$, $\hat{n}_i(\mathbf{r})$ are the unit normal vectors of triangles associated with the basis functions $\mathbf{f}_m$ and $\mathbf{g}_i$, respectively. Since U_{mn} V_{mp}, W_{im} involve the two-fold integrals and more time is needed to calculate B_{mn}, A_{ip}, the matrix filling is slightly more time consuming than the point matching method.

The corresponding matrix equations of (17)–(19) are as follows,

$$[B][H] = [U][H] + [V][E] \tag{20}$$

$$[A][E^{scat}] = [W][H] \tag{21}$$

$$[A][E] = [\tilde{E}^{inc}] + [A][E^{scat}] \tag{22}$$

To construct the FIM formulations, the matrices $[A]$ and $[B]$ are decomposed into two parts,

$$[B] = [B^D] + [B^C], \ [A] = [A^D] + [A^C] \tag{23}$$

where $[B^D]$ and $[A^D]$ are the diagonal matrices of $[B]$ and $[A]$, respectively, the remaining parts of corresponding matrices are $[B^C]$ and $[A^C]$. Using these decompositions of matrices $[B]$ and $[A]$, the FIM formulations can be obtained as follows

$$[H] = [B^D]^{-1} \left(([U] - [B^C])[H'] + [V][E] \right) \tag{24}$$

$$[E^{scat}] = [A^D]^{-1} \left(-[A^C][E^{',scat}] + [W][H] \right) \tag{25}$$

$$[E] = [E^{inc}] + [E^{scat}] \tag{26}$$

In the iteration process, the initial values are set to be $[E^{inc,(0)}] = [A^D]^{-1}[\tilde{E}^{inc}]$ and $[E^{inc}] = [A^D]^{-1} \left(-[A^C][E^{inc}] + [\tilde{E}^{inc}] \right)$.

3. NUMERICAL RESULTS

To verify and compare the 3D FIM formulations using the point matching and Galerkin's methods, the monostatic scattering from several 3D cavities are analyzed. The first cavity investigated is a 3D rectangular cavity shown as in Fig. 4.
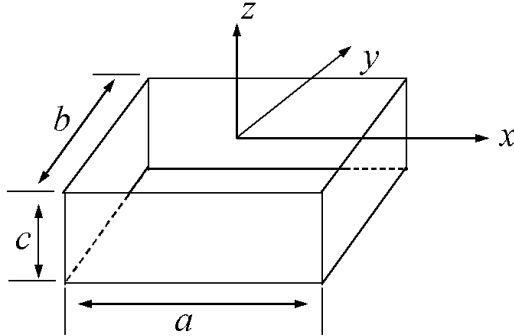

Figure 4. Geometry of the 3D rectangular Cavity.

Figures 5 and 6 show HH polarization ($\phi\phi$ polarization) and VV polarization ($\theta\theta$ polarization) backscatter patterns of the rectangular cavity with $a = 4\lambda$, $b = 4\lambda$ and $c = \lambda$, and $a = 4\lambda$, $b = 4\lambda$ and $c = 2\lambda$, respectively. The results obtained using the FIM and MoM are in good agreement when the incident angle is not very large, and some differences occur between the results obtained using the FIM and MoM for large incident angles. It should be noted that the MoM provides a complete solution including not only the contribution from the interior scattering but also the contributions from exterior scattering and rim diffraction. In contrast, the FIM provides only the contribution from the interior scattering. When the incident angle θ is not very large, the interior contribution is dominant over other contributions. If the incident angle is large, the contribution from the exterior scattering becomes important. Therefore, difference between the results obtained using the FIM and MoM is expected, especially for cavity with small aperture. The better results for the VV case is due to the less significant rim effect as compared to the HH polarization case. Since Kirchhoff approximation is utilized in the FIM formulation, better results are expected when the size of the aperture increases. Figure 7 shows the backscatter patterns for the rectangular cavity with $a = 5\lambda$, $b = 5\lambda$, $c = \lambda$. Better agreement between results obtained using the FIM and MoM can be observed, as compared to that in Fig. 7.
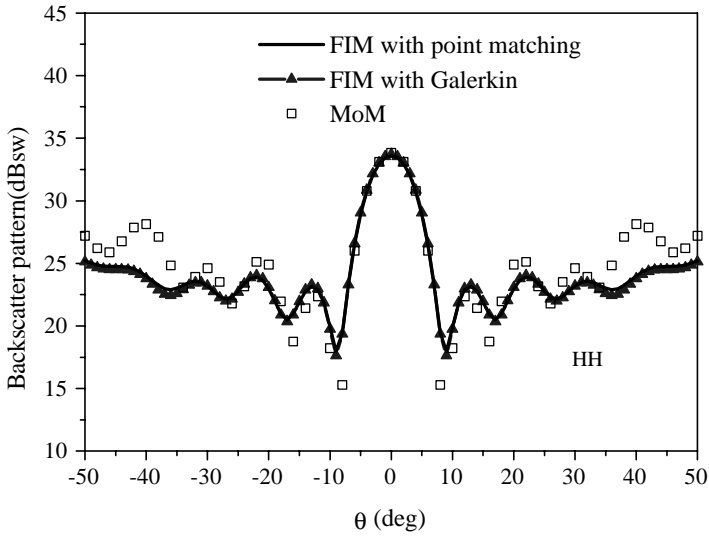
(a)
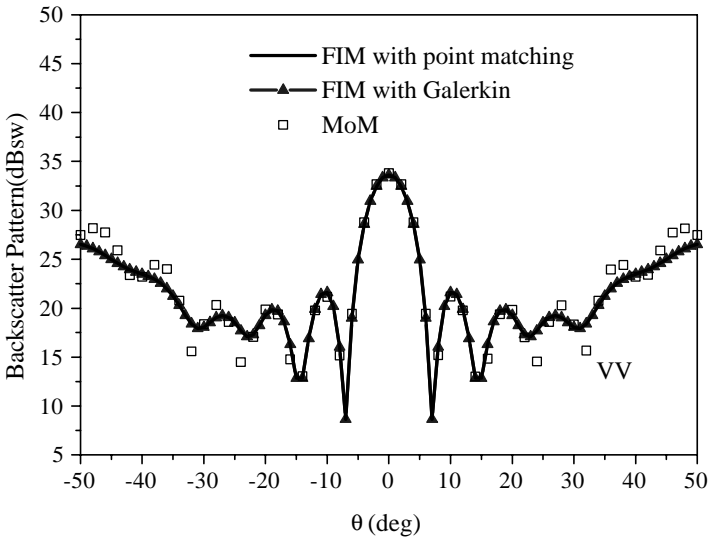
(b)

Figure 5. Backscatter patterns of a rectangular cavity with $a = 4\lambda$, $b = 4\lambda$, and $c = \lambda$ for $\phi = 0°$. (a) HH polarization. (b) VV polarization.
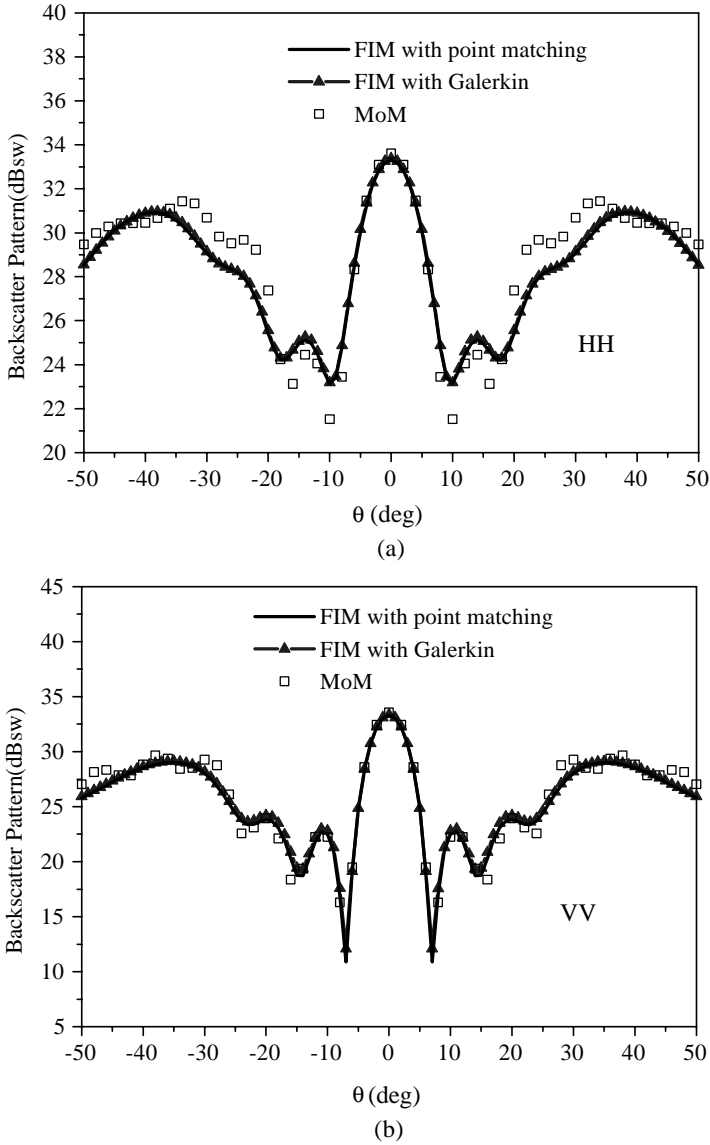
Figure 6. Backscatter patterns of a rectangular cavity with $a = 4\lambda$, $b = 4\lambda$ and $c = 2\lambda$ for $\phi = 0°$ (a) HH polarization. (b) VV polarization.
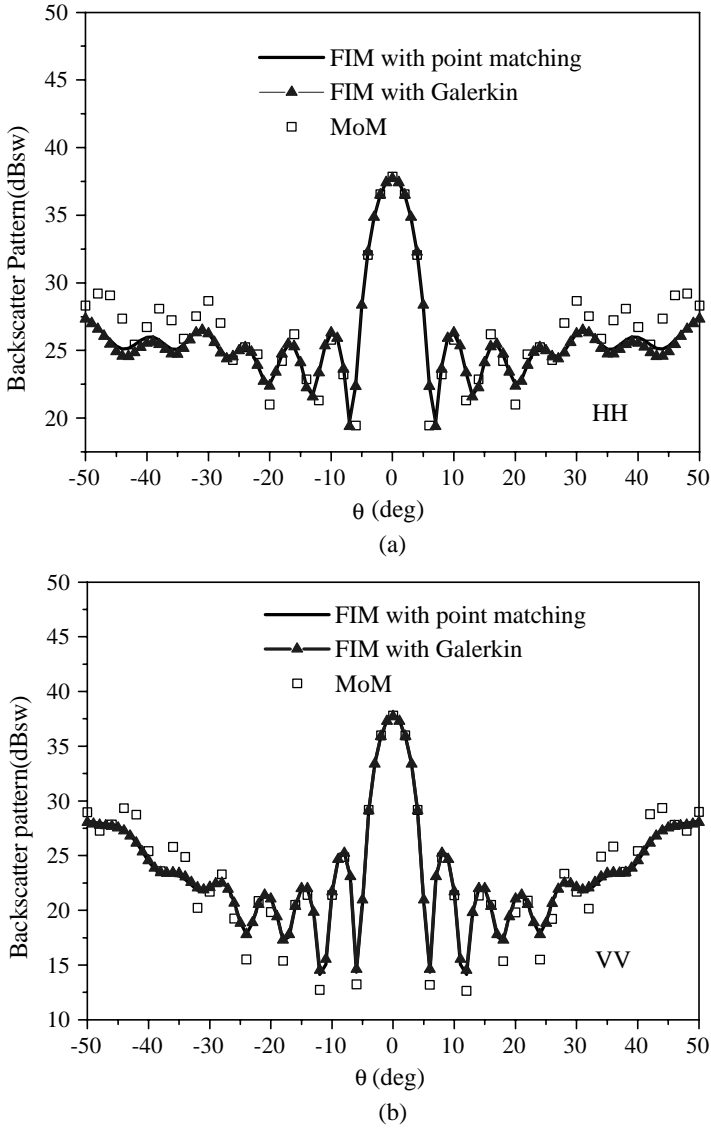
Figure 7. Backscatter patterns of a rectangular cavity with $a = 5\lambda$, $b = 5\lambda$, and $c = \lambda$ for $\phi = 0°$. (a) HH polarization. (b) VV polarization.
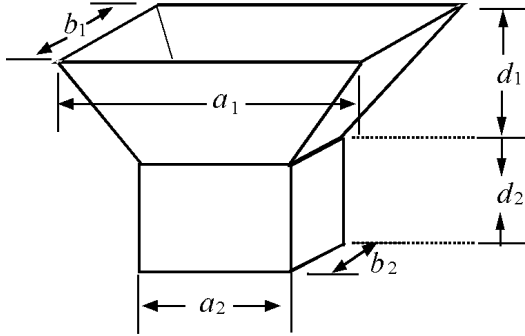
Figure 8. Geometry of 3D horn.

To check on the dependency of the testing procedures, numerical results obtained using the FIM with point matching and Galerkin's methods are also given in Figs. 5–7. It can be seen that excellent agreement is observed between the two testing procedures. This validates the point matching method for RWG basis function, which can result in a simpler FIM formulation.

The second cavity investigated is a metallic horn as shown in Fig. 8 with $a_1 = 4\lambda$, $b_1 = 4\lambda$, $d_1 = \lambda$ and $a_2 = 4\lambda$, $b_2 = 4\lambda$, $d_2 = \lambda$. Figure 9 shows the backscatter patterns of the metallic horn cavity for HH ($\phi\phi$) and VV ($\theta\theta$) polarizations. The results obtained using the FIM and MoM agree well for all angles concerned. It is also observed that the FIMs using the point matching and Galerkin's methods have almost same accuracy.

The last cavity investigated is a circular cavity with radius $r = 3\lambda$ and depth $d = \lambda$. Figure 10 shows the backscatter patterns of the circular cavity for both HH ($\phi\phi$) and VV ($\theta\theta$) polarizations. The results obtained using the FIM are compared to the results obtained using an in-house code based on the mode matching method, which has been verified to be correct and accurate for circular cavity modeling [22]. All results agreed well for all angles concerned. It is also observed that the results obtained using the FIMs with different testing procedures have almost same accuracy.

In all numerical experiments discussed above, the convergence criterion for all simulations requires that the root mean square difference of the quantities is less than 1%, which is rather strict for scattering analysis of the cavities. Table 1 gives the number of unknowns and average number of iterations (ANI) for all incident angles with different polarizations in all tested rectangular cavities. It shows that the convergence of the FIM is very fast for all cases. In
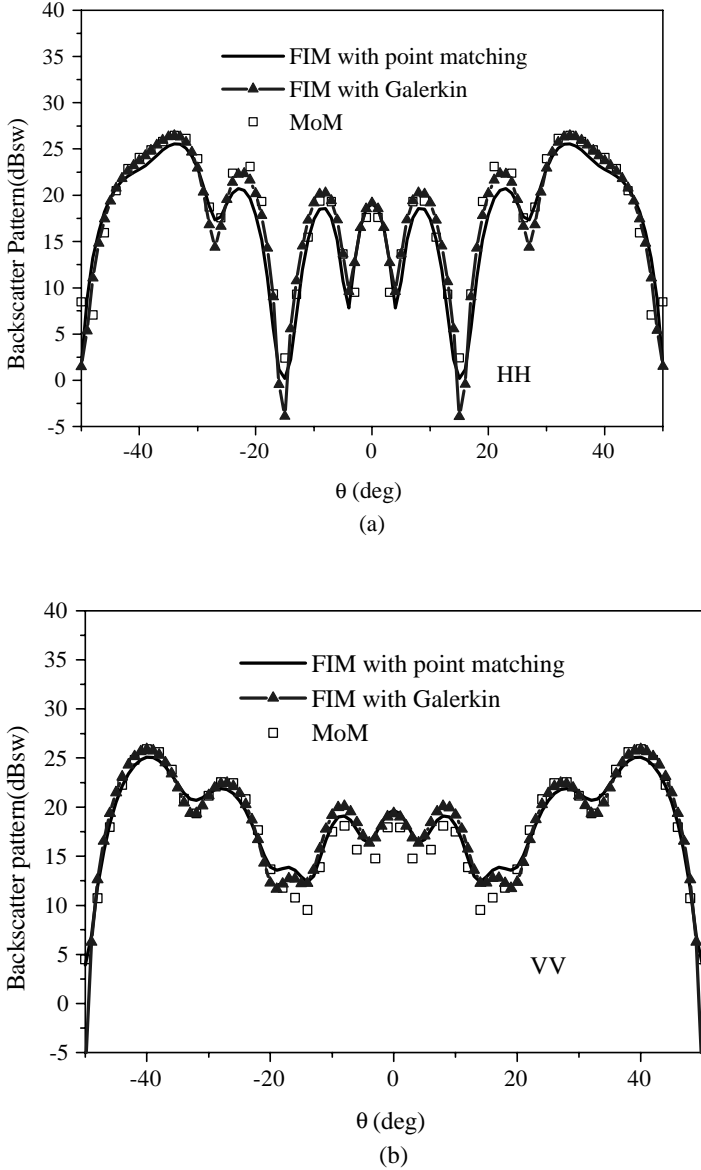
Figure 9. Backscatter patterns of rectangular horn with $a_1 = 4\lambda$, $b_1 = 4\lambda$, $a_2 = \lambda$, $b_2 = \lambda$, $d_1 = \lambda$, and $d_2 = \lambda$ for $\phi = 0°$. (a) HH polarization. (b) VV polarization.
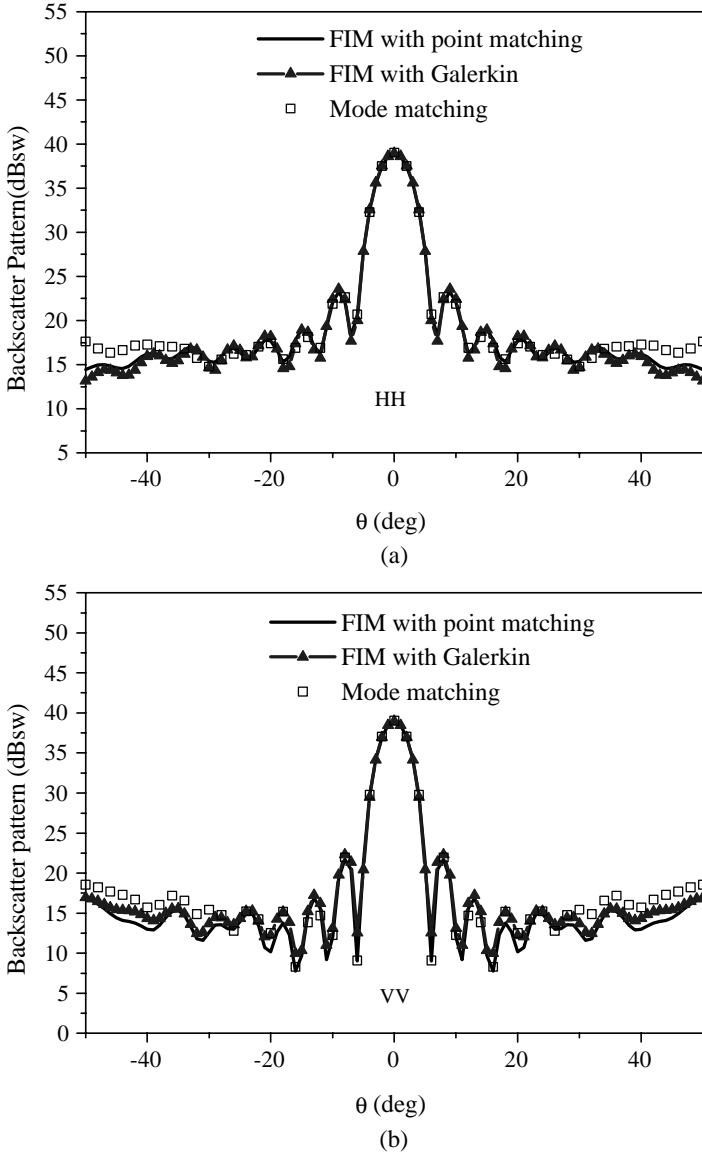
Figure 10. Backscatter patterns of circular cavity with radius $r = 3\lambda$ and depth $d = \lambda$ for $\phi = 0°$. (a) *HH* polarization. (b) *VV* polarization.

Table 1. The number of unknowns and average number of iterations for different sizes of rectangular cavities.

Rectangular Cavity size	Number of unknowns	Average number of iterations
$4\lambda \times 4\lambda \times \lambda$	4620	19
$5\lambda \times 5\lambda \times \lambda$	6320	20
$4\lambda \times 4\lambda \times 2\lambda$	9344	21
$7.5\lambda \times 7.5\lambda \times \lambda$	12030	17

particular, when the size of cavity increases, the ANI seems to remain almost the same. Similar convergence behaviour has also been observed for the horn and circular cavities.

4. CONCLUSIONS

3D field iterative method has been implemented using two different testing procedures, i.e., the point matching method and Galerkin's method, and has been verified by the simulation of backscattering from several different cavities. All test cases show that the FIM is accurate for large cavity and converges quite rapidly. The number of iterations appears to be somewhat independent of the size of cavity. The FIM using the point matching method is sufficiently accurate for large cavity modeling. This will keep the formulation of the 3D implementation of the FIM as simple as that of 2D. This also retains some advantages of the original FIM [13], such as, the FIM iterative procedure consists solely of vector inner products, and none of these matrices need to be inverted. Thus, the iterative solution process is directly applicable to high-speed vector processing computer systems and also to parallel processing systems.

ACKNOWLEDGMENT

APPENDIX A.

When the field point $\mathbf{r}''$ is an interior point in the cavity region D, as $\mathbf{r}''$ approaches to a point $\mathbf{r}$ on S_2, we need to exclude this point with a small half sphere having a small surface as depicted in Fig. A1.
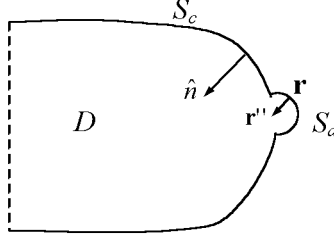

Figure A1. Geometry for a problem with the field point $\mathbf{r}$ being on cavity surface S_2.

$$
\hat{n}(\mathbf{r}) \times \int_S \mathbf{J}(\mathbf{r}') \times \nabla'G(\mathbf{r}'', \mathbf{r}')ds'
$$
$$
= \hat{n}(\mathbf{r}) \times \int_{S_a + S_C} \mathbf{J}(\mathbf{r}') \times \nabla'G(\mathbf{r}'', \mathbf{r}')ds' \qquad (A1)
$$

As $\mathbf{r}'' \to \mathbf{r}$, the integral over S_C goes to the second term on the right hand side of eq. (3). Let us now focus on the surface integral over S_a. On S_a, $R = |\mathbf{r}'' - \mathbf{r}'| = |\mathbf{r}'' - \mathbf{r}|$ is infinitesimal and therefore the phase factors in $G(\mathbf{r}'', \mathbf{r}')$ and $\nabla'G(\mathbf{r}'', \mathbf{r}')$ are negligible. By using the mean value for fields at $\mathbf{r}$ and with

$$
\nabla'G(\mathbf{r}'', \mathbf{r}') = \frac{1 + jk_0R}{4\pi R^2} e^{-jk_0R}\hat{R} \text{ and } \hat{R} = \frac{\mathbf{r}'' - \mathbf{r}'}{|\mathbf{r}'' - \mathbf{r}'|},
$$

we obtain

$$
\lim_{\mathbf{r}'' \to \mathbf{r}} \hat{n}(\mathbf{r}) \times \int_{S_a} \mathbf{J}(\mathbf{r}') \times \nabla'G(\mathbf{r}'', \mathbf{r}')ds'
$$
$$
= \lim_{R \to 0} \hat{n}(\mathbf{r}) \times (\mathbf{J}(\mathbf{r}) \times \nabla'G(\mathbf{r}'', \mathbf{r})) \cdot 2\pi R^2
$$
$$
= \lim_{R \to 0} \frac{1 + jk_0R}{4\pi R^2} e^{-jk_0R} \cdot 2\pi R^2 \mathbf{J}(\mathbf{r}) = \frac{1}{2}\mathbf{J}(\mathbf{r})
$$

Thus, the validity of equation (3) is established. The same idea can be found in evaluating the residue of a divergent integral for scalar wave [20].

REFERENCES

1. Harrington, R. F. and J. R. Mautz, "A generalized network formulation for aperture Problems," *IEEE Trans. Antennas Propagat.,* Vol. 24, 870–873, Nov. 1976.

2. Liang, C. H. and D. K. Cheng, "Electromagnetic field coupled into a cavity with a slot-aperture under resonant conditions," *IEEE Trans. Antennas Propagat.,* Vol. 30, 664–672, 1982.

3. Ling, H., R. Chou, and S. W. Lee, "Shooting and bouncing rays: Calculating RCS of an arbitrary cavity," *IEEE Trans. Antennas Propagat.,* Vol. 37, No. 2, 194–205, Feb. 1989.

4. Burkholder, R. J. and P. H. Pathak, "High-frequency electromagnetic scattering by open-ended waveguide cavities," *Radio Sci.,* Vol. 26, 211–218, Jan–Feb. 1991.

5. Basteiro, F. O., J. L. Rodriguez, and R. J. Burkholder, "An iterative physical optics approach for analyzing the electromagnetic scattering by large open-ended cavities," *IEEE Trans. Antennas Propagat.,* Vol. 43, No. 4, 356–361, April 1995.

6. Jin, J. M. and J. L. Volakis, "A finite elementboundary integral formulation for scattering by three-dimensional cavity-backed apertures," *IEEE Trans. Antennas Propagat.,* Vol. 39, 97–104, Jan. 1991.

7. Jin, J. M., *The Finite Element Method in Electromagnetics,* Wiley, New York, 1993.

8. Jin, J. M., "Electromagnetic scattering from large, deep, and arbitrarily-shaped open cavities," *Electromagn.,* Vol. 18, No. 1, 3–34, Nov. 1998.

9. Liu, J. and J. M. Jin, "A special higher order finite-element method for scattering by deep cavities," *IEEE Trans. Antennas Propagat.,* Vol. 48, 697–703, May 2000.

10. Liu, J., E. Dunn, P. Baldensperger, and J. M. Jin, "Computation of radar cross section of jet engine inlet," *Microwave Opt. Tech. Lett.,* Vol. 33, No. 5, 322–325, June 2002.

11. Wang, T. M. and H. Ling, "Electromagnetics scattering from three-dimensional cavities via a connection scheme," *IEEE Trans. Antennas Propagat.,* Vol. 39, 1505–1513, Oct. 1991.

12. Wang, T. M. and H. Ling, "A connection scheme on the problem of EM scattering from arbitrary cavities," *J. Electromagn. Waves Appl.,* Vol. 5, No. 3 301–314, 1991.

13. Reuster, D. D. and G. A. Thiele, "A field iterative method for computing the scattering electric field at the apertures of large

perfectly conducting cavities," *IEEE Trans. Antennas Propagat.,* Vol. 43, No. 3, 286–290, Mar. 1995.

14. Wang, C. F., Y. B. Gan, T. H. Chien, and L. W. Li, "On the field iterative method for modeling of two-dimensional large aperture open-ended cavity," *J. Electromagn. Waves Appl.,* Vol. 17, No. 8, 113–1130, 2003.

15. Wang, C. F., Y. B. Gan, and G. A. Thiele, "Field iterative method based on an accurate equivalent model of cavity," Technical Report No.: TL/EM/03/004, Temasek Laboratories, National University of Singapore, Feb. 2003.

16. Wang, C. F., Y. B. Gan, and G. A. Thiele, "An accurate equivalent model for field iterative method," *IEEE APS Int. Symp. Dig.,* Vol. 2, 338–341, 2003.

17. Rao, S. M., D. R. Wilton, and A. W. Glisson, "Electromagnetic scattering by surface of arbitrary shape," *IEEE Trans. Antennas Propagat.,* Vol. 30, 409–418, May 1982.

18. Harrington, R. F., *Time Harmonic Electromagnetic Fields,* 106–110, McGraw-Hill, New York, 1961.

19. Balanis, C. A., *Advanced Engineering Electromagnetics,* Wiley, New York, 1989.

20. Chew, W. C., *Waves and Fields in Inhomogeneous Media,* Van Nostand Reinhold, New York, 1990, Reprinted by IEEE Press, 1995.

21. Harrington, R. F., *Field Computation by Moment Methods,* Macmillan, New York, 1968.

22. Lee, C. S. and S. W. Lee, "RCS of a coated circular waveguide terminated by a perfect conductor," *IEEE Trans. Antennas Propagat.,* Vol. 35, 391–398, April 1987.

Chao-Fu Wang received the B.Sc. degree in mathematics from the Henan Normal University, Xinxiang, China, in 1985, the M.Sc. degree in applied mathematics from the Hunan University, Changsha, China, in 1989, and the Ph.D. degree in electrical engineering from the University of Electronic Science and Technology of China, Chengdu, China, in 1995, respectively. From 1987 to 1996, he was a Lecturer, and then an Associate Professor of the Department of Applied Mathematics at the Nanjing University of Science and Technology (NUST). Since February 1996, he has been an Associate Professor of the Department of Electronic Engineering at the NUST. From 1996–1999, he was a Postdoctoral Research Fellow in the Center for Computational Electromagnetics (CCEM), University of Illinois

at Urbana-Champaign (UIUC). From 1999–2001, he was a Research Fellow in the Department of Electrical and Computer Engineering, National University of Singapore (NUS). He is currently a Research Scientist and Project Leader in the Temasek Laboratories, NUS. His current research interests include fast algorithms for computational electromagnetics, scattering and antenna analysis, ferrite components and their analysis, MMIC design and simulation.

Yuan Xu received the B.S., M.S. degrees in mathematics from Suzhou University, P. R. China, and Ph.D. degrees in electromagnetic theory and microwave technology from Nanjing University of Science and Technology, P. R. China, in 1988, 1991, and 2001, respectively. He is currently a Research Scientist in the Temasek Laboratories, National University of Singapore. From 1991 to 1999, he was with Department of Applied Mathematics, Nanjing University of Science and Technology. From May 1999 to September 2000, he was a research assistant in Department of Electric Engineering, City University of Hong Kong. His research interests include computational electromagnetics, integral equation methods, and analysis of large-scale electromagnetic radiation and scattering problem.

Yeow-Beng Gan received the B.Eng. (Hons) and M.Eng. degrees in electrical engineering from the National University of Singapore, Singapore, in 1989 and 1994, respectively. He has been with the DSO National Laboratories (formerly the Defense Science Organization) since 1989, and was primarily responsible for the build-up of technical capabilities in the analysis and design of antennas in DSO. He became a Principal Member of Technical Staff in 1998, in the area of electromagnetics and antennas. In May 2001, he was seconded to the Temasek Laboratories, National University of Singapore, where he is currently a Principal Research Scientist. His research interests include periodic arrays for antennas and radomes, wave physics, computational electromagnetics, and modeling of composite materials.